A DFT Request for the Band Gap, NBO Analysis, and Global Reactivity of the Doped Metallofullerenes and their Complexes with H_2 Molecules

Kadhim, Mustafa M.*[+•]
Research Center, Kut University College, Kut, Wasit, IRAQ

Mohammadi Aghdam, Sarvin
Department of Chemistry, Payame Noor University, P. O. Box: 19395-3697 Tehran, I.R. IRAN

Azizi, Baya
Medical Laboratory Sciences Department, College of Health Sciences, University of Human Development, Sulaymaniyah, IRAQ

Ahmadi, Sheida; Poor Heravi, Mohammad Reza
Department of Chemistry, Payame Noor University, P. O. Box: 19395-3697 Tehran, I.R. IRAN

Ebadi, Abdol Ghaffar
Department of Agriculture, Jouybar Branch, Islamic Azad University, Jouybar, I.R. IRAN

Rahmani, Zahra*[+]
Department of Chemistry, Tabriz Branch, Islamic Azad University, Tabriz, I.R. IRAN

ABSTRACT: *In this theoretical report we are focused on the substituent effects of titanium dopants on the band gap, NBO, and global reactivity of $C_{20-n}Ti_n$ metallofullerenes (n = 1 - 5), at DFT. The $C_{18}Ti_{2-2}$ metallofullerene is found as the most stable analog with the highest band gap, in which carbon atoms are replaced by Ti dopants in the equatorial location, separately. The charge on carbon atoms of C_{20} is estimated roughly zero, while the high positive charge on the $C_{16}Ti_{4-2}$ surface prompts this metallofullerene for hydrogen storage. The positive charge on Ti heteroatoms and the negative charge on their adjacent C atoms implies that these sites can be able to be influenced more readily by nucleophilic and electrophilic reagents, correspondingly. The electronic transitions are usually classified according to the orbitals engaged or the involved specific parts of the metallofullerene. Common types of electronic transitions in organic compounds are "π–π*", "n–π*" and "π* (acceptor) – π (donor)". Fascinatingly, the charge transfer (CT) tack places via the suitable overlapping among $\sigma_{C—Ti}$ bonding's orbital along with $\sigma^*_{C—Ti}$ anti-bonding's orbital of $C_{20-n}Ti_n$ metallofullerenes. For example, the NBO analysis of $C_{19}Ti_1$ metallofullerene points out higher CT energy of $\sigma_{C—Ti} \rightarrow \sigma^*_{C—Ti}$ (16.31 kcal/mol) with respect to $\sigma_{C—Ti} \rightarrow \sigma^*_{C—C}$ (0.63 kcal/ mol).*

* *To whom correspondence should be addressed.*
+ *E-mail: Mustafa_kut88@yahoo.com ; z.1401rahmani@gmail.com*
● *Other Address: Research Center, Al-Turath University College, Baghdad, IRAQ*
● *Research Center, Al-Farahidi University, Baghdad, IRAQ*
1021-9986/2023/3/835-852 18/$/6.08

The reactivity of metallofullerenes can be affected by the number and topology of the substituted dopants. Based on these results we infer that metallofullerenes are a potential material for hydrogen storage with high capacity and the driving force for reactivity of them is the relief of π-curvature strain and leads $sp^2 \rightarrow sp^3$ hybridized atoms.

KEYWORDS: *Metallofullerene; Titanium; Heteroatom; Band gap; Reactivity.*

INTRODUCTION

Encapsulation and substitution of carbon atoms by heteroatoms have been an object for experimental and computational investigations expected to understand the stability, structural, chemical reactivity, and electronic and magnetic possessions of the nanostructures [1-3]. The carbon forms contain graphite, graphene, fullerene, carbon nanotube, cyclacene, acene, polyacene, cyclophenacene, nanographene, nanosheet, nanocone and nanocage [4-6]. Graphite consists of graphene layers. The stable C_{60} icosahedral structure is a graphitic hollow cage containing twelve pentagons with no restriction of hexagons. Contrary to C_{60}, dodecahedron $\mathbf{C_{20}}$ fullerene consists of twelve pentagons without a hexagon ring, resulting in an extreme curvature. This structure as the smallest hollow cage is the most strained fullerene and it is a promising candidate for high-temperature superconductors, because of its larger electron-phonon coupling than stable C_{60}. Nevertheless, recognition of a very short-lived $\mathbf{C_{20}}$ hollow cage has been achieved *via* de-bromination of $\mathbf{C_{20}Br_{20}}$ in the gas phase [7]. As a result of the high reactivity as well as low stability of $\mathbf{C_{20}}$, the geometrical electronic of $\mathbf{C_{20}}$, comes from experimental to theoretical research in the gas media.

Despite Ti-decorated B_{38} and B_{40} fullerenes that have been obtained as the first experimentally full-boron cages, hydrogen storage of the designed transition metal for example titanium atoms at hexagon and heptagon rings of these fullerenes has been explored *via* DFT calculations [8]. Experimental and theoretical investigations have revealed that titanium clusters significantly improve hydrogen storage properties [9]. Moreover, the Density Functional Theory (DFT) results predict the stability from $\mathbf{C_{20}}$ to its substitutional, endohedral, and exohedral derivatives to perform "superatom" which can be substitutional, exo, and endohedrally stabilized by releasing the strain energy, metal ion encapsulation and hydrogen adsorption, respectively. Some reports have been focused on Ti-metallofullerenes [10,11]. Here, we are focused on the electronic effect, NBO's study, AIM charge, and MEP analysis of $\mathbf{C_{20\text{-}n}Ti_n}$ analogs in which titanium atom(s) is an efficient hydrogen storage media for the metallofullerenes (Fig.1).

COMPUTATIONAL METHODS

Metallofullerenes is optimized by B3LYP, M06-2X/6-311+G* and B3LYP, M06-2X/AUG-cc-pVTZ [12-14]. To evolution shape and energy of the FMOs, the NBO calculations [15] are carried out at various methods and basis sets including B3LYP/AUG-cc-pVTZ, M06-2X/6-311++G** and B3PW91/6-311++G** [16]. The AIM charge and MEP map are obtained, individually. The nucleophilicity index, N, is calculated as $N = E_{HOMO(Nu)} - E_{HOMO(TCNE)}$, where tetracyanoethylene (TCNE) is chosen as the reference [17]. The global electrophilicity, ω, is calculated using $\omega = (\mu^2 / 2\eta)$, where μ is the chemical potential ($\mu = (E_{HOMO} + E_{LUMO}) / 2$) and η is the global hardness ($\eta = (E_{LUMO} - E_{HOMO}) / 2$) [17]. Also, χ is the absolute electronegativity ($\chi = -\mu$), S is the global softness ($S = 1 / 2\eta$) and ΔN_{max} is the maximum electronic charge of C_{20} and $C_{20\text{-}n}Ti_n$ metallofullerenes ($\Delta N_{max} = -\mu / \eta$) [17].

RESULTS AND DISCUSSION

FMOs & $\Delta E_{HOMO\text{-}LUMO}$

The FMOs are recognized as one of the initial approaches to characterize molecular interactions. Their shapes indicate the ability to donate and accept the electron respectively. The $\Delta E_{HOMO\text{-}LUMO}$ determines the chemical stability of the molecule. The FMO Eigenvalues are useful for computing various global chemical reactivity indices that predict the relative stability and reactivity of the molecules (Fig. 2) [19-23].

The FMO electron density of the scrutinized structures is mainly localized at their external surfaces. In metallofullerenes, most of the part of HOMOs are located over titanium heteroatoms whereas the LUMOs are

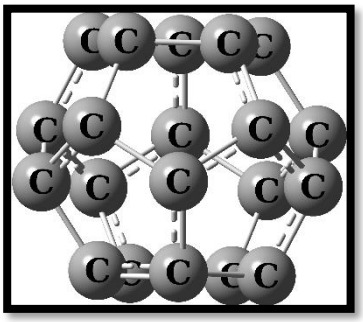

C_{20}

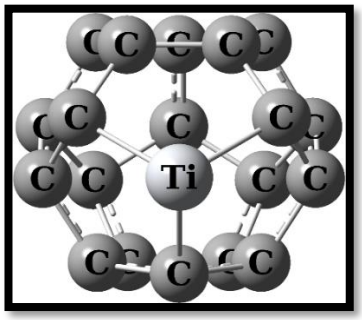

$C_{19}Ti_1$

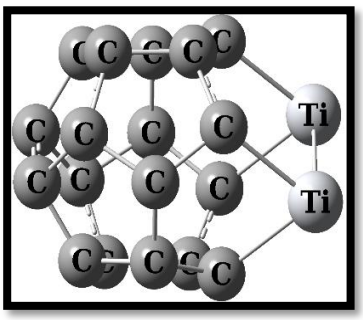

$C_{18}Ti_{2\text{-}1}$

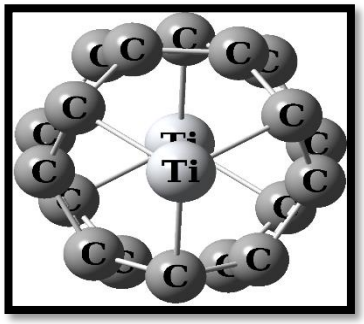

$C_{18}Ti_{2\text{-}2}$

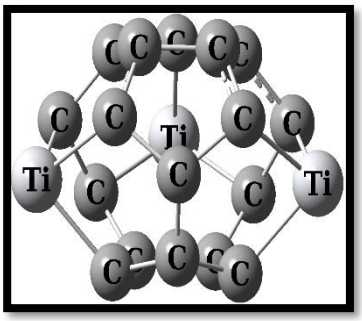

$C_{17}Ti_3$

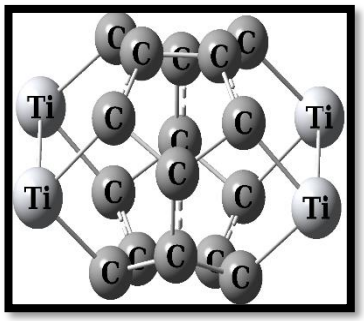

$C_{16}Ti_{4\text{-}1}$

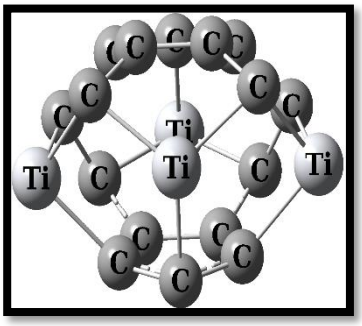

$C_{16}Ti_{4\text{-}2}$

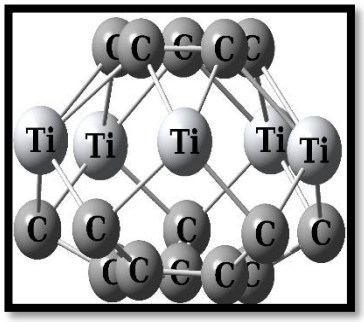

$C_{15}Ti_5$

Fig. 1: The geometries of C_{20} and $C_{20\text{-}n}Ti_n$ metallofullerenes, at B3LYP/AUG-cc-pVTZ.

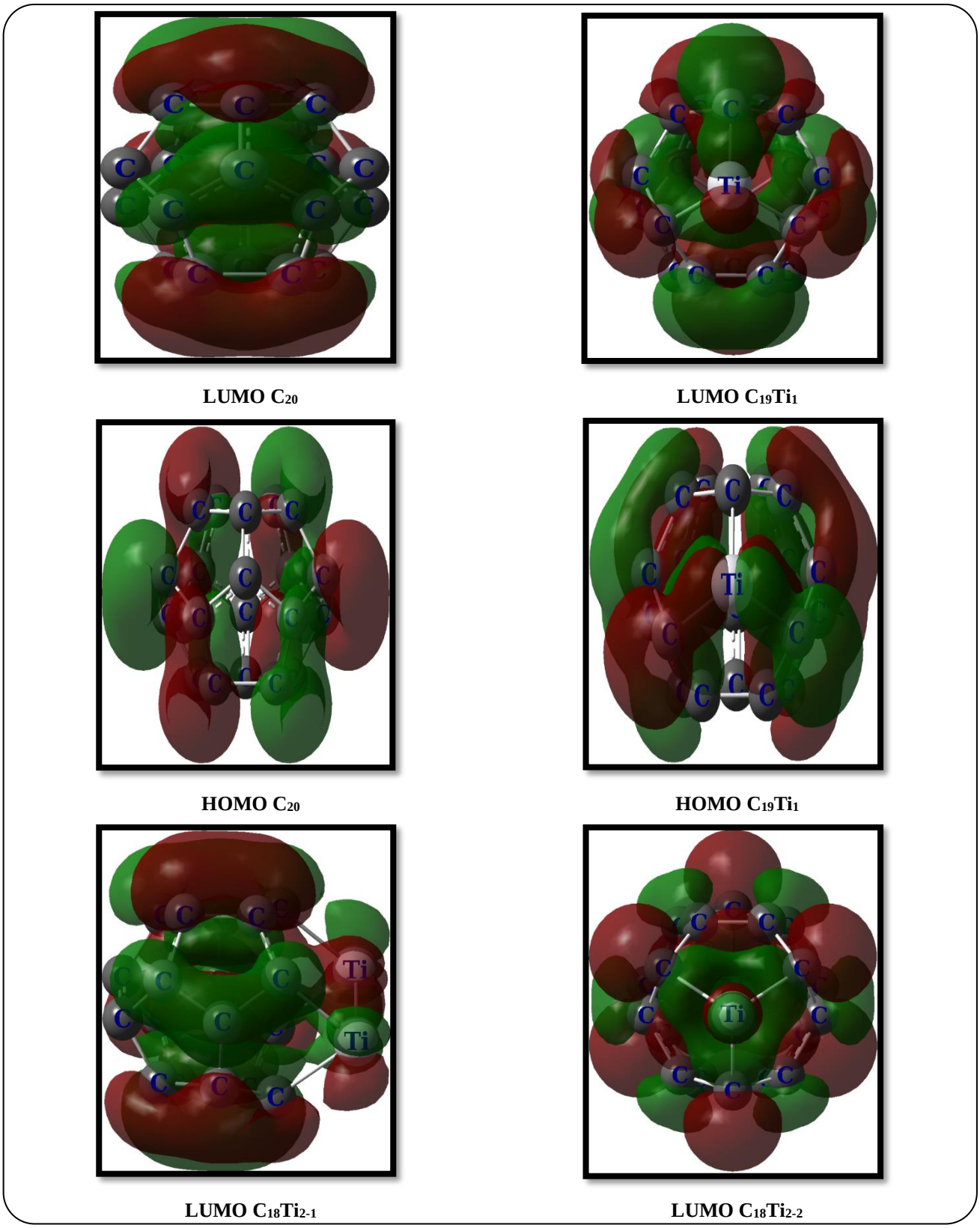

Fig. 2: The frontier molecular orbital shapes including the highest occupied molecular orbital (HOMO) and the lowest unoccupied molecular orbital (LUMO) of C_{20} and $C_{20-n}Ti_n$ metallofullerenes, at B3PW91/6-311++G**.

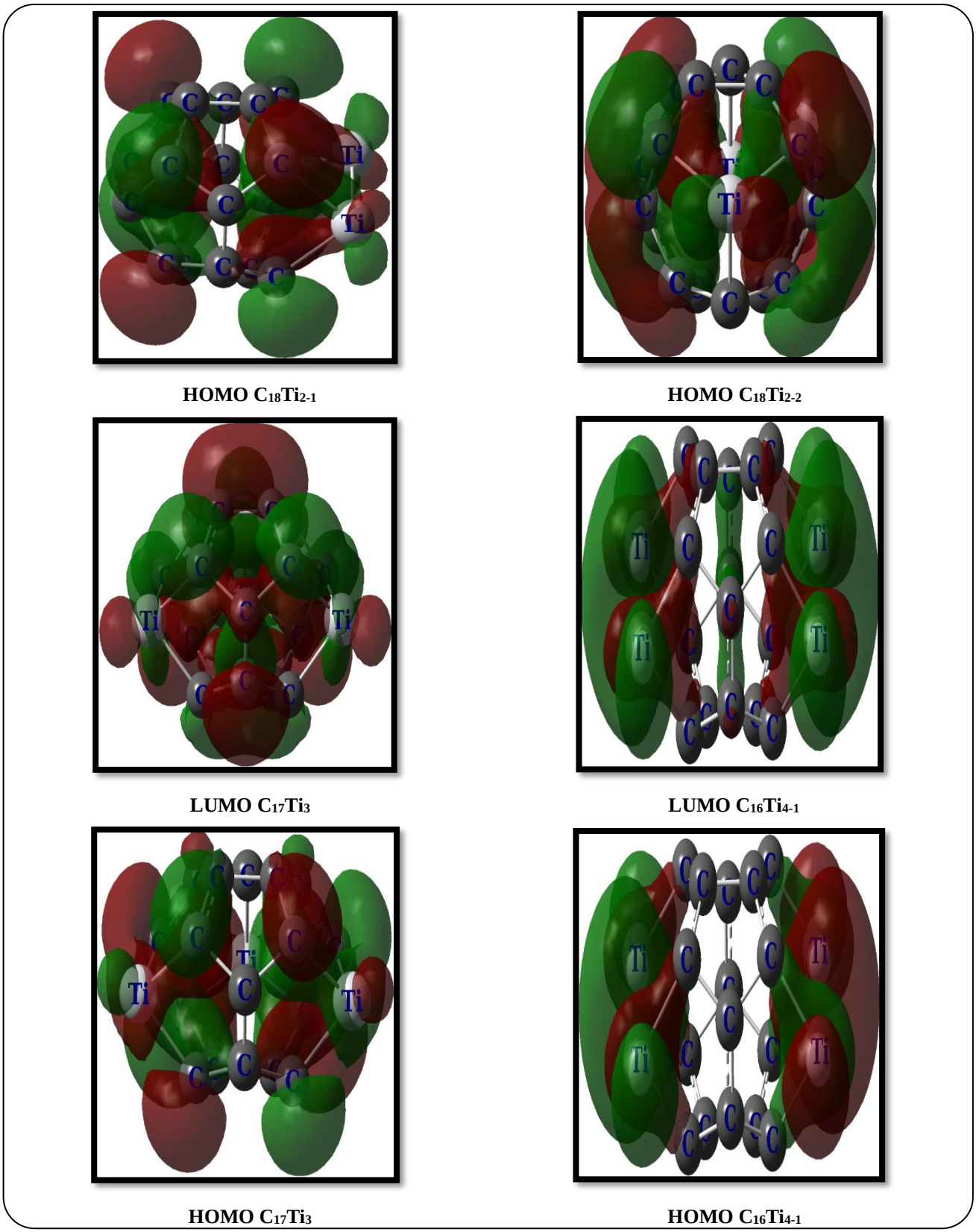

Fig. 2: The frontier molecular orbital shapes including the highest occupied molecular orbital (HOMO) and the lowest unoccupied molecular orbital (LUMO) of C_{20} and $C_{20-n}Ti_n$ metallofullerenes, at B3PW91/6-311++G**. ( )

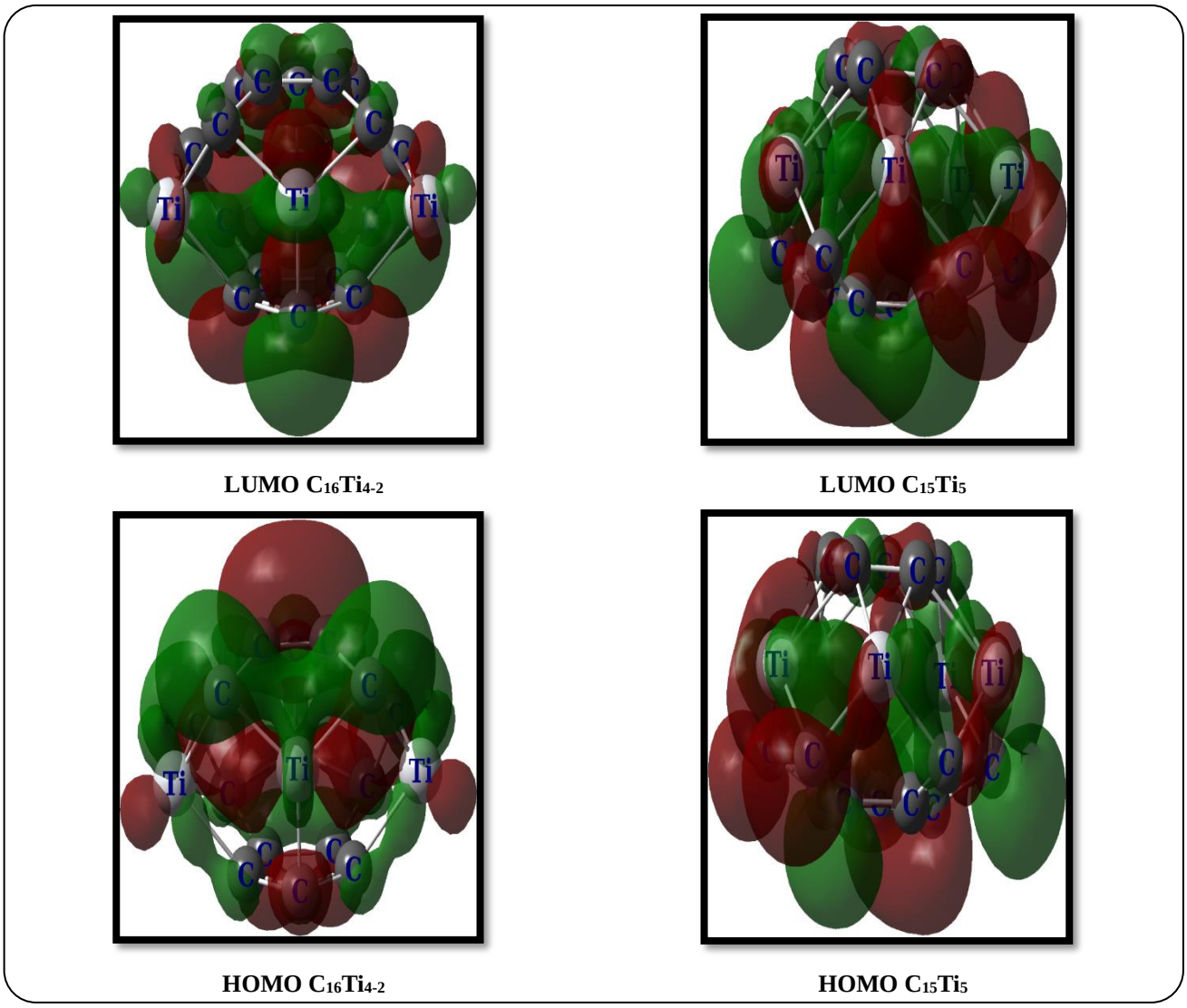

Fig. 2: The frontier molecular orbital shapes including the highest occupied molecular orbital (HOMO) and the lowest unoccupied molecular orbital (LUMO) of C_{20} and $C_{20-n}Ti_n$ metallofullerenes, at B3PW91/6-311++G**. ( )

delocalized over the whole C–C bonds. The HOMO–LUMO excitations in these molecules imply an electron density transfer from Ti atoms to C atoms and redistribution of the charge density on the fullerene surface. The most important point is the selection of methods and basis sets in theoretical studies. However, the main difficulty deals with the study of FMOs and the use of these results to calculate reactivity indexes. The FMO's energy makes these metallofullerenes as the suitable conductor with the narrowest $\Delta E_{HOMO-LUMO}$. Apart from **$C_{19}Ti_1$**, **$C_{18}Ti_{2-1}$**, **$C_{16}Ti_{4-1}$** and **$C_{15}Ti_5$** that their HOMO-LUMO energy splitting ($\Delta E_{HOMO-LUMO}$ or band gap) is smaller than that of **C_{20}**, the band gap of **$C_{18}Ti_{2-2}$** and **$C_{17}Ti_3$** metallofullerenes is higher than that of pure cage (Table 1).

Thus, the electron is easier to remove and transfer from HOMO to LUMO potential surface of **$C_{19}Ti_1$**, **$C_{18}Ti_{2-1}$**, **$C_{16}Ti_{4-1}$** and **$C_{15}Ti_5$** than that of the unsubstituted cage. Furthermore, two substituted separately titanium heteroatoms of **$C_{18}Ti_{2-2}$** increase the band gap and lead to improved conductivity. The FMO's energy Eigen values along with their gaps indicated that **$C_{18}Ti_{2-2}$** metallofullerene is the most stable in the gaseous state because of its largest gap among the studied nanocages as well as it is least reactive than those having smaller gaps. Also, **$C_{16}Ti_{4-1}$** metallofullerene is considered as the least stable species in a gaseous state because of its narrowest gap among the studied nanocages as well as it is predicted

Table 1: The FMO energies (E_{HOMO} and E_{LUMO} in a.u.), along with their band gap ($\Delta E_{HOMO-LUMO}$ in eV) calculated for C_{20} and $C_{20-n}Ti_n$ metallofullerenes.

Species	E_{HOMO} [a, (b), [c]]	E_{LUMO} [a, (b), [c]]	$\Delta E_{HOMO-LUMO}$ [a, (b), [c]]
C_{20}	-0.20134, (-0.21055), [-0.20455]	-0.13054, (-0.12567), [-0.13351]	1.93, (2.31), [1.93]
$C_{19}Ti_1$	-0.19088, (-0.19973), [-0.19339]	-0.13080, (-0.12471), [-0.13239]	1.63, (2.04), [1.66]
$C_{18}Ti_{2-1}$	-0.17181, (-0.18118), [-0.17282]	-0.11933, (-0.11876), [-0.12053]	1.43, (1.70), [1.42]
$C_{18}Ti_{2-2}$	-0.20158, (-0.20960), [-0.20397]	-0.10947, (-0.10433), [-0.10927]	2.51, (2.86), [2.58]
$C_{17}Ti_3$	-0.17113, (-0.17994), [-0.17244]	-0.09820, (-0.09353), [-0.09903]	1.98, (2.35), [2.00]
$C_{16}Ti_{4-1}$	-0.13224, (-0.14344), [-0.13330]	-0.09851, (-0.10025), [-0.09848]	0.92, (1.18), [0.95]
$C_{16}Ti_{4-2}$	-0.16664, (-0.17302), [-0.16765]	-0.09672, (-0.08749), [-0.09587]	1.90, (2.33), [1.95]
$C_{15}Ti_5$	-0.15776, (-0.16144), [-0.15826]	-0.10461, (-0.09762), [-0.10486]	1.45, (1.74), [1.45]

*At [a]B3LYP/AUG-cc-pVTZ, [b]M06-2X/6-311++G** and [c]B3PW91/6-311++G**.*

as the most reactive species in chemical reactions than those having wider gaps. The electronegativity difference among Ti and C atoms (Ti = 1.54 and C = 2.55) induces π-electron polarization from titanium toward its adjacent carbons and causes increasing of band gap in **$C_{19}Ti_1$**, **$C_{18}Ti_{2-2}$**, **$C_{17}Ti_3$** and **$C_{16}Ti_{4-2}$** compared to **$C_{18}Ti_{2-1}$**, **$C_{16}Ti_{4-1}$** and **$C_{15}Ti_5$** which are more conductive than **C_{20}**. The occupancy of one carbon atom by one titanium atom, improves the π-ring current (Fig. 2). Interestingly, band gap of the **$C_{18}Ti_{2-2}$**, and **$C_{16}Ti_{4-2}$** metallofullerenes with respect to their corresponding isomers (**$C_{18}Ti_{2-1}$** and **$C_{16}Ti_{4-1}$**) is increased considerably because of the appearance of some electronic states from the separated titanium sites; *i.e.* the electronic property of the metallofullerenes is sensitive to number and arrangement of the Ti-dopants. Another words, **$C_{18}Ti_{2-2}$** and **$C_{16}Ti_{4-2}$** heterofullerenes easily permit the promotion of unpaired electrons from the d^2-orbitals of Ti-substituted dopant to the π*-orbitals of their bonded C atoms. Evidently, due to the existence of electronic repulsions of titanium heteroatoms, this strong π-ring current slightly is vanished in the **$C_{18}Ti_{2-1}$** and **$C_{16}Ti_{4-1}$**. From band gap view point, the former species (**$C_{18}Ti_{2-2}$** and **$C_{16}Ti_{4-2}$**) benefit from strong π-bond conjugation across Ti—C bonds, while the latter species (**$C_{18}Ti_{2-1}$** and **$C_{16}Ti_{4-1}$**) suffer from electronic repulsion and weak π-bond conjugation across Ti—Ti bonds in the corresponding cages. For either **$C_{18}Ti_{2-1}$** or **$C_{16}Ti_{4-1}$** configuration, the highest positive spin density is localized on the substituted titanium dopants and the carbon atom bears a very small spin density (see Fig. 2). This may imply that titanium heteroatoms are more reactive in **$C_{18}Ti_{2-1}$** and **$C_{16}Ti_{4-1}$** configurations than those in the other configurations (**$C_{18}Ti_{2-2}$** and **$C_{16}Ti_{4-2}$**) toward a radical addition.

AIM charge and MEP map

The AIM theory defines the spatial volume of an atom in a molecule by electron density topology analysis [24]. An atom's spatial volume is defined as the volume enclosed by zero-flux surfaces of the electron density. The zero-flux surfaces are the union of all points where $\nabla\rho \cdot n = 0$ (ρ is the electron density and n is the unit vector normal to the surface). These volumes are nonspherical and do not overlap to each other. Once the atom's spatial volume is determined, it's AIM charge is obtained by integrating electron density over the volume. The electron density includes the information on each atoms' electronegativities, therefore AIM charge does take the atom's electronegativity into account. The AIM atomic charge approves the hydrogen storage possibility of the doped metallofullerene, nanostructures because of enlarging binding energy of the adsorbed H_2 molecules on surfaces of them. Here, to probe the possible application of **C_{20}** and **$C_{20-n}Ti_n$** metallofullerenes as hydrogen storage, the AIM charge is accomplished at M06-2X/6-311++G** level of theory (Fig. 3).

Substituent effects are another important concept in chemistry since they induce changes in electron density and thus affect physico-chemical properties of molecules. Without a doubt, slight alterations in type of the substituted atom as dopant and topology of metallofullerene either cap or equatorial position can make possible change of value,

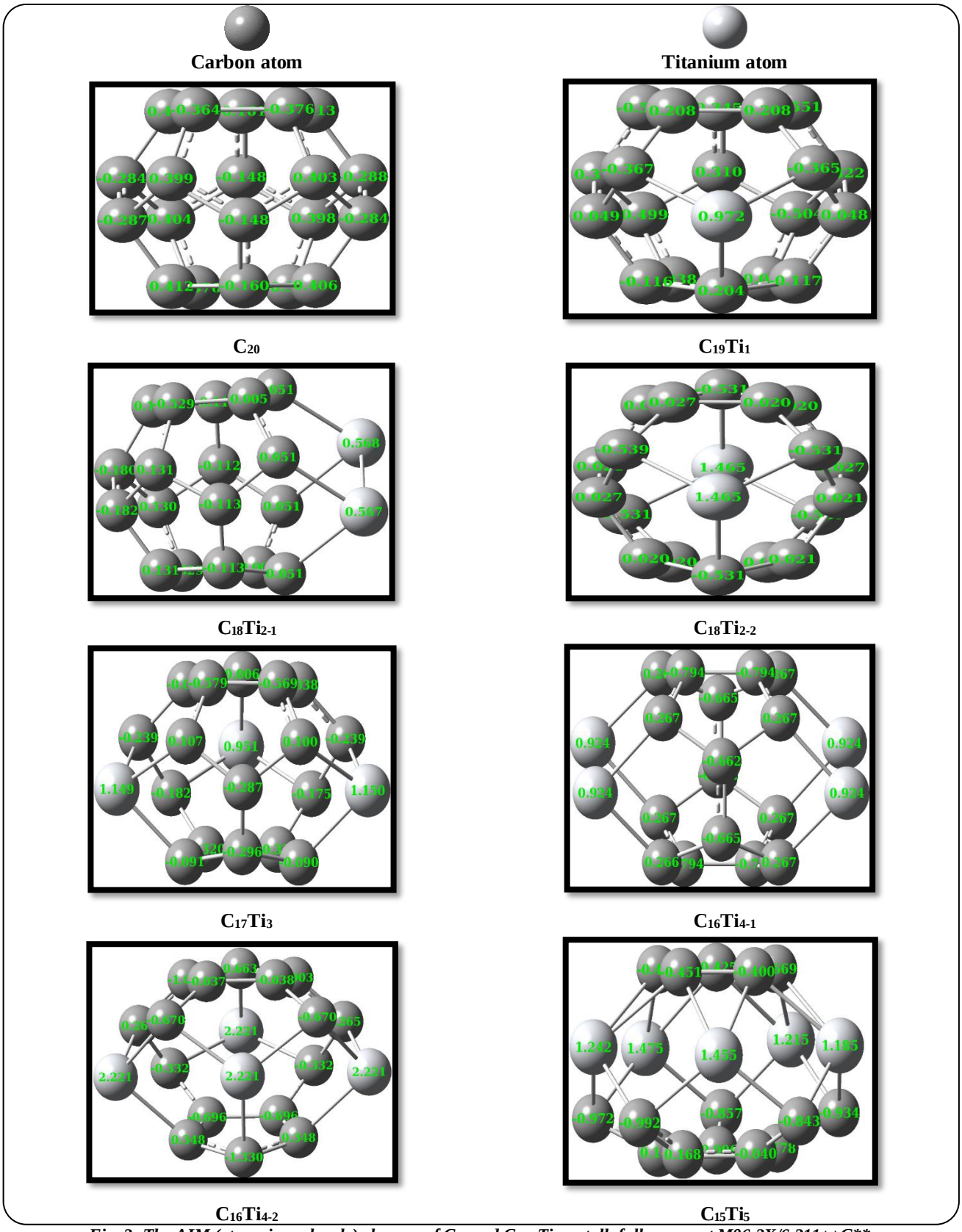

*Fig. 3: The AIM (atoms in molecule) charges of C_{20} and $C_{20-n}Ti_n$ metallofullerenes, at M06-2X/6-311++G**.*

sign of charge, point group, electrophilic and nucleophilic's site, *etc*. The range of AIM charge distribution on carbon atoms of pristine **C_{20}** is varied from -0.148 to +0.412. The charge trend is rationalized by the quality of the σ bonds of Ti—Ti. Thus, **$C_{18}Ti_{2\text{-}1}$** and **$C_{16}Ti_{4\text{-}1}$** metallofullerenes having one and two Ti—Ti single bonds is carried out the lowest positive charge on the corresponding Ti heteroatoms (+0.568 and +0.924, respectively). On the other site, **$C_{18}Ti_{2\text{-}2}$** and **$C_{16}Ti_{4\text{-}2}$** metallofullerenes having six and twelve Ti—C single bonds and no Ti—Ti bonds is carried out the highest positive charge on the corresponding Ti heteroatoms (+1.465 and +2.221, respectively). Next comes **$C_{15}Ti_5$** structure having twenty Ti—C single bonds but no C=C double bonds between Ti heteroatoms in the equatorial position, which is carried out differently with positive charges on its titanium dopants from +1.185 to +1.475. The presence of the neighboring C=C double bonds to the Ti—C single bonds, however, is suggested to be the main reason for the stronger resonance of **$C_{18}Ti_{2\text{-}2}$** and **$C_{16}Ti_{4\text{-}2}$** metallofullerenes relative to the corresponding **$C_{18}Ti_{2\text{-}1}$** and **$C_{16}Ti_{4\text{-}1}$** isomers. Thus, the π-electron delocalization within the Ti—C=C—Ti bonds improves the overall π-electron delocalization and ring current in equatorial position, which results in higher degree of charge transfer. The point charges upon the material surface can improve the storage capacity since they increase the binding energy of hydrogen to the surface [25]. Here, **C_{20}** with the least positive charge is found as the worst candidate for hydrogen storage; while the investigated metallofullerenes especially **$C_{16}Ti_{4\text{-}2}$** analogue with the maximum positive charge on Ti—dopants are suitable candidate [25]. To create the MEP energy data easy to render, a color spectrum, with red as the lowest MEP energy value and blue as the highest, is utilized to convey the varying strengths of the MEP energy values. It is a tool for realizing and guessing the reactive behavior of a molecule. There are many applications of the MEP in the fields such as molecular recognition, hydrogen bonding and understanding of variety of physiochemical properties related to molecular interactions. In any particular region around a molecule, the sign of the MEP depends upon whether the effects of the nuclei or electrons are dominant. It is a key to assessing its reactivity there. Herein, these values (*a.u.*) are calculated in the range of -1.540e-2 *a.u.* (deepest red) to 1.540e-2 *a.u.* (deepest blue) (Fig. 4).

The extension of the positive MEP around the titanium heteroatoms and the regions of negative MEP around the carbon atoms gives the same conclusion obtained by Froudakis about the nature of the intramolecular charge transfer in hydrogen adsorption as found by the orientation of the molecular dipole moment (Fig. 5).

Each Ti— -unit can bind up to 5 H_2 molecules with an average adsorption energy of 0.182 eV/H_2. Additional 10 H_2 molecules can be absorbed into one **$C_{18}Ti_2$** metallofullerene, resulting in hydrogen capacities of 6.07 wt% with a high adsorption energy of 0.365 eV/H_2 (Fig. 6).

While the **$C_{15}Ti_5$** metallofullerene substituted with 5 Ti— units can store 25 H_2 molecules, the hydrogen gravimetric density (the hydrogen storage capacity) reaches up to 10.72 wt% with an average adsorption energy of 0.912 eV/H_2. Based on these results we infer that **$C_{18}Ti_2$**, **$C_{17}Ti_3$**, **$C_{16}Ti_4$**, and **$C_{15}Ti_5$** metallofullerenes are potential materials for hydrogen storage with high capacity and might motivate active experimental efforts in designing hydrogen storage media. Also, **$C_{18}Ti_2$**, **$C_{17}Ti_3$**, **$C_{16}Ti_4$**, and **$C_{15}Ti_5$** metallofullerenes with the average adsorption energy of 0.365, 0.547, 0.730, and 0.912 eV/H_2, respectively, satisfy the requirements of DOE.

NBO analysis

In order to recognize various second order interactions among electron donors and electron acceptors, NBO analysis is completed on the simplest **$C_{19}Ti_1$** metallofullerene (Table 2).

The sp^2 hybrid is found from occupancy between 1.514 for $\sigma_{C7-Ti20}$ with $0.789*sp^{24.36}d^{0.02}+0.613*sp^{0.05}d^{2.76}$ hybrid *vs*. 1.929 electrons for $\sigma_{C19-Ti20}$ bonding orbitals with $0.863*sp^{2.44}d^{0.00}+0.505*sp^{0.28}d^{1.93}$ hybrid. The $sp^{24.36}$ hybrid on C_7 has 3.94% s and 96.00% p; also the $sp^{2.44}$ hybrid on C_{19} has 29.04% s and 70.95% p-character. The $sp^{0.05}d^{2.76}$ hybrid on Ti_{20} has 26.28% s, 1.23% p and 72.45% d-character and so the $sp^{0.28}d^{1.93}$ hybrid on Ti_{20} has 31.07% s, 8.83% p and 60.04% d-character. These bonding orbitals have 62.38% C_7 and 37.62% Ti_{20} character in $sp^{24.36}d^{0.02}$ and $sp^{0.05}d^{2.76}$ hybrids and so 74.44% C_{19} and 25.56% Ti_{20} character in $sp^{2.44}d^{0.00}$ and $sp^{0.28}d^{1.93}$ hybrids. Therefore, Ti_{20} has a lower percentage of NBO and shows a lower polarization coefficient than C_7 and C_{19} atoms in bonding sigma bonds. The 0.789 and 0.613 values in $\sigma_{C7-Ti20}$ bond and the values of 0.863 and 0.505 in $\sigma_{C19-Ti20}$ bond

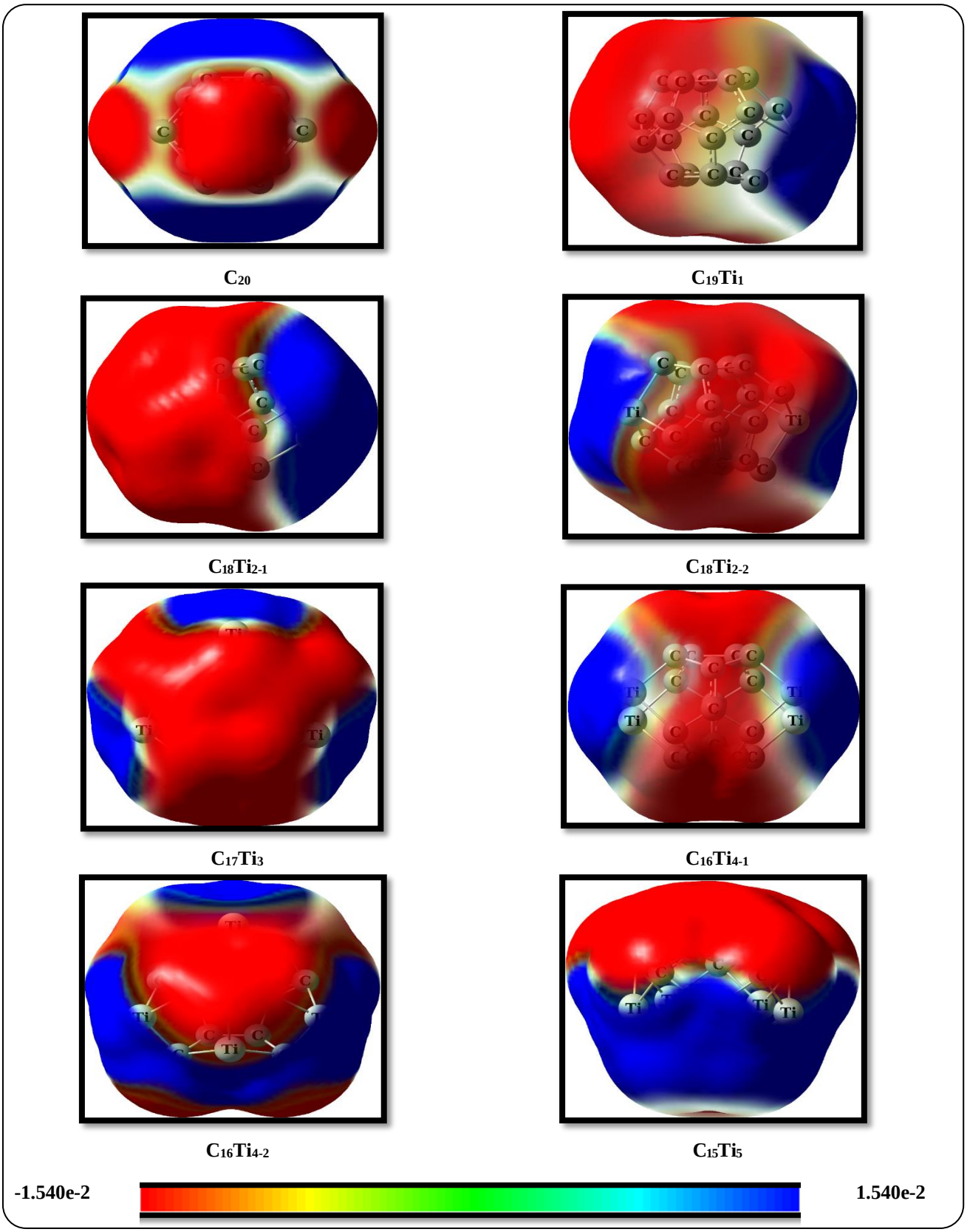

Fig. 4: The MEP (molecular electrostatic potential) maps of C_{20} and $C_{20-n}Ti_n$ metallofullerenes.

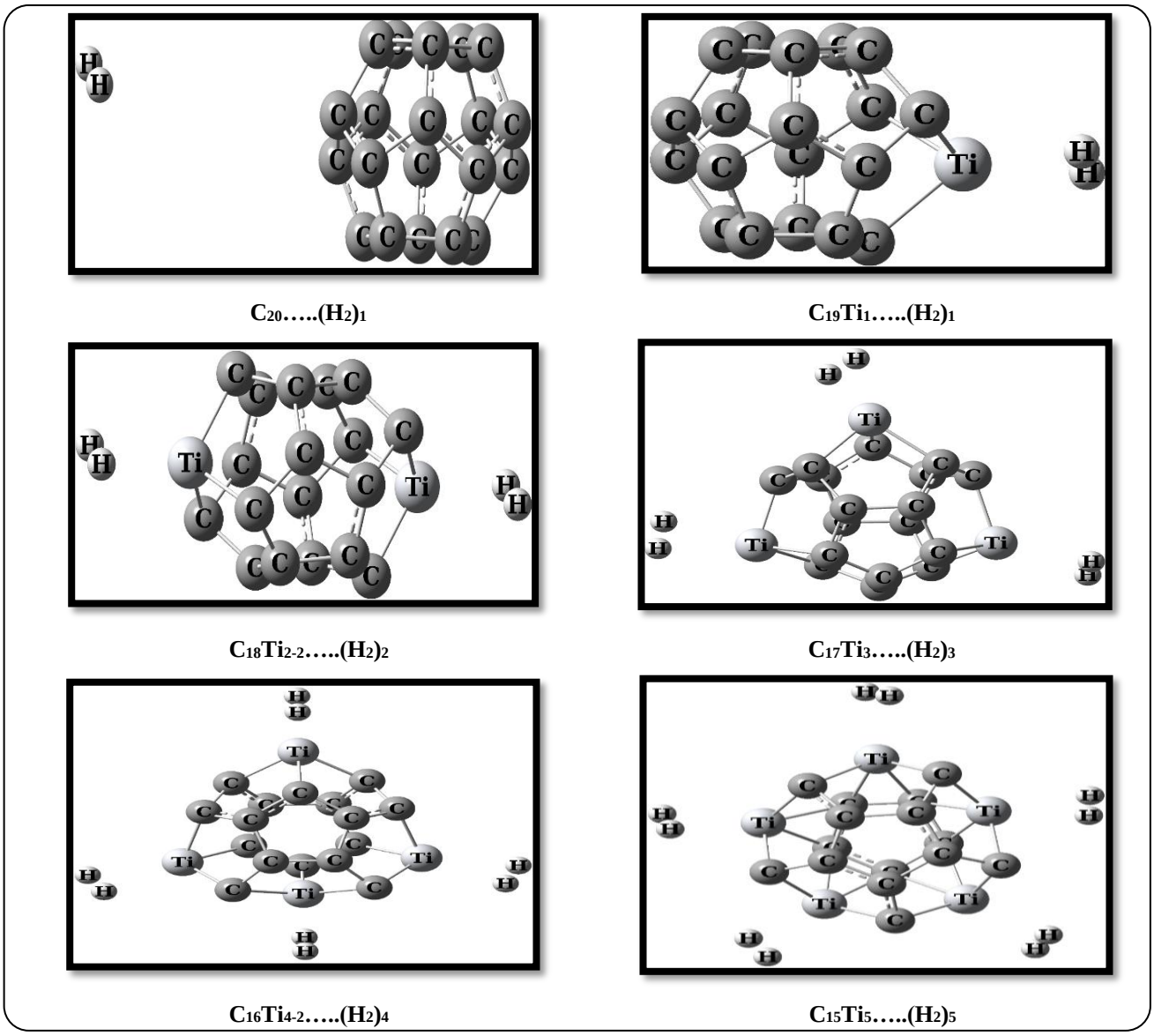

Fig. 5: The optimized structures for hydrogen adsorption.

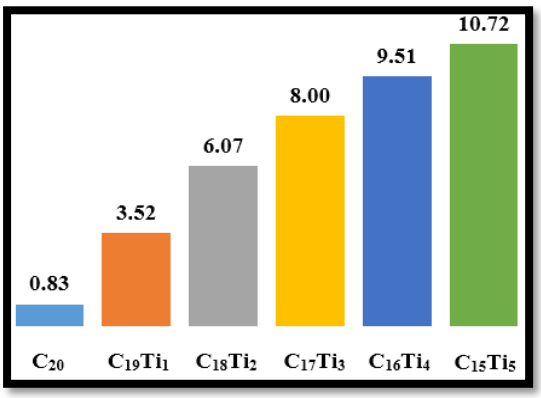

Fig. 6: The hydrogen gravimetric density (wt%) of the scrutinized metallofullerenes.

exhibit polarization coefficients. It means that the other coefficients are non-polarization. More polarization coefficient suggests more electron-rich atoms in the formation of one bond. In fact, the intramolecular interaction is developed through suitable overlap among the bonding orbital of $\sigma_{C7—Ti20}$ with an anti-bonding orbital of $\sigma^*_{C8—C9}$ and $\sigma^*_{C19—Ti20}$ which results in the occurred CT from $\sigma_{C7—Ti20}$ as a donor to $\sigma^*_{C8—C9}$ and $\sigma^*_{C19—Ti20}$ as acceptor, with an increasing of its occupancy. The important interaction energy ($E^{(2)}$) is found from the bonding orbital of $\sigma_{C7—Ti20}$ to the anti-bonding orbitals of $\sigma^*_{C8—C9}$ and $\sigma^*_{C19—Ti20}$ and their related energies are 0.63 and 16.31 kcal mol^{-1}, respectively (Table 3).

Table 2: NBO (natural bond orbital) results showing the occupancy, formation of Lewis and non-Lewis orbital's the valence hybrids of the intramolecular bonds in $C_{19}Ti_1$, at B3PW91/6-311++G**.

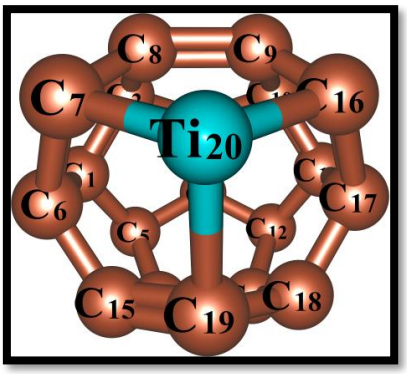

Bond (A-B)	Occup.	ED_A (%)	ED_B (%)	NBO	s (%)	p (%)	d (%)
$\sigma_{C7—Ti20}$	1.514	62.38	37.62	$0.789*sp^{24.36}d^{0.02}+0.613*sp^{0.05}d^{2.76}$	3.94, 26.28	96.00, 1.23	0.06, 72.45
$\sigma_{C19—Ti20}$	1.929	74.44	25.56	$0.863*sp^{2.44}d^{0.00}+0.505*sp^{0.28}d^{1.93}$	29.04, 31.07	70.95, 8.83	0.02, 60.04

Table 3: The calculated second order perturbation energies $E^{(2)}$ in kcal/mol corresponding to the most important charge transfer interactions (donor-acceptor) in $C_{19}Ti_1$, at B3PW91/6-311++G**.

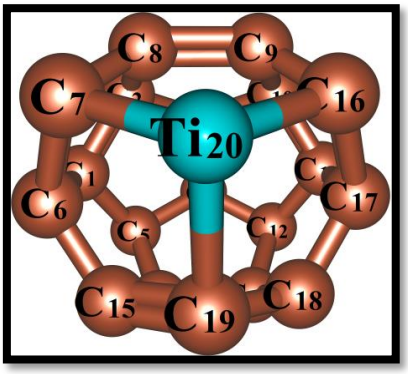

Donor NBO (i)	Acceptor NBO (j)	$E^{(2)}$ (kcal mol^{-1})	E(j) – E(i) (*a.u.*)	F (i,j) (*a.u.*)
$\sigma_{C7—Ti20}$	$\sigma^*_{C8—C9}$	0.63	0.65	0.021
$\sigma_{C7—Ti20}$	$\sigma^*_{C19—Ti20}$	16.31	0.39	0.079

The lowest $E^{(2)}$ (0.63 kcal mol^{-1}) as a criterion of thermodynamically stabilization energy, for the lowest electron density transfer is considered for the weakest intramolecular interaction of $\sigma_{C7—Ti20} \rightarrow \sigma^*_{C8—C9}$. While the highest value (16.31 kcal mol^{-1}) is considered the strongest intramolecular interaction of $\sigma_{C7—Ti20} \rightarrow \sigma^*_{C19—Ti20}$.

Global reactivity

Titanium causes diverse changes of reactivity in $\mathbf{C_{20-n}Ti_n}$ metallofullerenes compared to $\mathbf{C_{20}}$ (Table 4).

Two substituted Ti atoms individually in $\mathbf{C_{18}Ti_{2-2}}$ metallofullerene lead to the lowest value of N, S, and ΔN_{max} as well as the highest among the substituted structures. In contrast, four substituted Ti atoms individually in $\mathbf{C_{16}Ti_{4-1}}$ metallofullerene lead to the highest value of N, S, χ, μ and ΔN_{max} along with the lowest η. Therefore, $\mathbf{C_{18}Ti_{2-2}}$ is the most chemically stable species, while $\mathbf{C_{16}Ti_{4-1}}$ is the most chemically reactive species. The driving force for reactivity of the substituted metallofullerene is the relief of curvature strain and leads $sp^2 \rightarrow sp^3$ hybridized atoms. Henceforth,

Table 4: The reactivity parameters including N, ω, μ, η, χ, S and ΔNmax (all in eV) calculated for C20 and C20-nTin metallofullerenes, at M06-2X/6-311++G**.

Species	N	ω	μ	η	χ	S	ΔN_{max}
C_{20}	3.73	4.53	-4.57	2.31	4.57	0.22	1.98
$C_{19}Ti_1$	4.03	4.77	-4.41	2.04	4.41	0.24	2.16
$C_{18}Ti_{2\text{-}1}$	4.53	4.90	-4.08	1.70	4.08	0.29	2.40
$C_{18}Ti_{2\text{-}2}$	3.76	3.18	-4.27	2.86	4.27	0.17	1.49
$C_{17}Ti_3$	4.56	2.94	-3.72	2.35	3.72	0.21	1.58
$C_{16}Ti_{4\text{-}1}$	5.56	4.68	-3.32	1.18	3.32	0.43	2.82
$C_{16}Ti_{4\text{-}2}$	4.75	2.70	-3.54	2.33	3.54	0.21	1.52
$C_{15}Ti_5$	5.07	3.58	-3.52	1.74	3.52	0.29	2.03

the reactivity of metallofullerenes can be affected by the number and topology of the substituted dopants.

CONCLUSIONS

DFT calculations reveal that band gap, AIM charge distribution, MEP, NBO analysis, N, ω and other reactivity indexes are affected by n and the array of the substituted dopants. The calculated band gap of **$C_{18}Ti_{2\text{-}2}$** (2.51, 2.86 and 2.58 eV) and **$C_{16}Ti_{4\text{-}2}$** (1.90, 2.33 and 1.95 eV) is estimated wider than that of **$C_{18}Ti_{2\text{-}1}$** (1.43, 1.70 and 1.42 eV) and **$C_{16}Ti_{4\text{-}1}$** (0.92, 1.18 and 0.95 eV, at B3LYP/AUG-cc-pVTZ, M06-2X/6-311++G** and B3PW91/6-311++G**, respectively). Then, **$C_{18}Ti_{2\text{-}2}$** is found as the best insulated and the weakest conductive metallofullerene. Isolating Ti—dopants using double bonds of C=C is a relevant approach for achieving more kinetic stability of **$C_{18}Ti_{2\text{-}2}$** and **$C_{16}Ti_{4\text{-}2}$** structures (about two times) than the corresponding isomers; **$C_{18}Ti_{2\text{-}1}$** and **$C_{16}Ti_{4\text{-}1}$** that suffer from electronic repulsion of Ti—Ti bonds. However, due to some local distortion of the atomic structure, the distribution of the wave function is slightly delocalized around the titanium dopants instead of carbon atoms. For example, for either **$C_{16}Ti_{4\text{-}1}$** or **$C_{16}Ti_{4\text{-}2}$** configuration, the highest positive spin density is localized on the equatorial titanium atoms and the capped carbon atoms bear a very small spin density. This may imply that titanium atoms are more reactive than the capped carbon atoms toward a radical addition in both isomers of **$C_{16}Ti_{4\text{-}1}$** and **$C_{16}Ti_{4\text{-}2}$**. The **$C_{18}Ti_{2\text{-}2}$** and then **$C_{16}Ti_{4\text{-}1}$** metallofullerenes include the lowest and the most chemical reactivity among the surveyed structures. The substituted doping leads to positive AIM atomic charge on Ti heteroatoms of **$C_{20\text{-}n}Ti_n$** metallofullerenes with the highest value of +2.221 in **$C_{16}Ti_{4\text{-}2}$**. According to Froudakis's findings and respecting positive charge distribution, it seems that **C_{20}** with the least positive charge and **$C_{16}Ti_{4\text{-}2}$** metallofullerene with the most positive charge on its Ti atoms are the worst and the best candidate for hydrogen storage, correspondingly. Two substituted Ti atoms individually in the most chemically stable species; **$C_{18}Ti_{2\text{-}2}$** lead to the lowest value of N (3.76 eV), S (0.17 eV) and ΔN_{max} (1.49 eV) as well as the highest η (2.86 eV). In contrast, two homo bonds of Ti—Ti in the least chemically stable species; **$C_{16}Ti_{4\text{-}1}$** causes to the highest value of N (5.56 eV), S (0.43 eV), χ (3.32 eV), μ (-3.32 eV) and ΔN_{max} (2.82 eV) along with the lowest η (1.18 eV). Investigation on the intramolecular interaction of **$C_{19}Ti_1$** metallofullerene indicates $\sigma_{C—Ti} \rightarrow \sigma^*_{C—Ti}$ as the strongest stabilization energy (16.31 kcal mol^{-1}) compared to $\sigma_{C—Ti} \rightarrow \sigma^*_{C—C}$ as the weakest stabilization energy (0.63 kcal mol^{-1}). Hence, the significant electron delocalization occurs due to one Ti-substitution in this species.

Received : Nov.. 7, 2022 ; Accepted : Feb. 20, 2023

REFERENCES

[1] (a) Nazar Ali Z, Ahmadi S A, Ghazanfari D, Sheikhhosseini E, Razavi R., Investigation of Flutamide@ethyleneimine as Drug Carrier by Nanocone and Nanotube Theoretically, *Iran. J. Chem. Chem. Eng. (IJCCE)*, **41(10)**: 3275–3286 (2022). Doi: 10.30492/ijcce.2021.542408.5014.

(b) Tavakoli S, Ahmadi S A, Ghazanfari D, Sheikhhosseini E., Theoretical Investigation of Functionalized Fullerene Nano Carrier Drug Delivery of Fluoxetine, *J. Indian Chem. Soc.*, **99**: 100561 (2022). doi.org/10.1016/j.jics.2022.100561.

(c) Najibzade Y., Sheikhhosseini E., Akhgar M.R., Ahmadi S.A., Absorption of Tranylcypramine on C_{60} Nanocage: Thermodynamic and Electronic Properties, *Pakistan J. Pharma. Sci.*, **35**: 815(2022). doi.org/10.36721/PJPS.2022.35.3.REG.815-818.1.

(d) Razavi R., Kaya S., Zahedifar M., Ahmadi S.A., Simulation and Surface Topology of Activity of Pyrazoloquinoline Derivatives as Corrosion Inhibitor on the Copper Surfaces, *Sci. Repor.* (2021). doi.org/10.1038/s41598-021-91159-6.

[2] (a) Koohi M., Bastami H., Structure, Stability, MEP, NICS, Reactivity, and NBO of Si—Ge Nanocages Evolved from C_{20} Fullerene at DFT, *Monatsh. Chem. – Chem. Month.* **151**:693–710 (2020).

(b) Koohi M., Ghavami M., Haerizade B.N., Zandi H., Kassaee M.Z., Cyclacenes and Short Zigzag Nanotubes with Alternating Ge—C Bonds: Theoretical Impacts of Ge on the Ground State, Strain, and Band Gap, *J. Phys. Org. Chem.* **27**:735–746 (2014).

(c) Baei M.T., Koohi M., Shariati M., Characterization of C_{20} Fullerene and its Isolated $C_{20-n}Ge_n$ Derivatives (n = 1-5) by Alternating Germanium Atom(S) in Equatorial Position: A DFT Survey, *Heteroatom Chem.* **29**: e21410–21423 (2018).

(d) Soleimani Amiri S., Koohi M., Mirza B., Characterizations of B, and N Heteroatoms as Substitutional Doping on Structure, Stability, and Aromaticity of Novel Heterofullerenesevolvedfrom the Smallest Fullerene Cage C_{20}: A Density Functional Theory Perspective, *J. Phys. Org. Chem.* **29**:514–522 (2016).

(e) Koohi M., Soleimani Amiri S., Haerizade B.N., Substituent Effect on Structure, Stability and Aromaticity of Novel $B_nN_mC_{20-(n+m)}$ Heterofullerenes, *J. Phys. Org. Chem.* **30**: e3682–3692 (2017).

[3] (a) Soleimani-Amiri S., Koohi M., Azizi Z., Characterization of Nonsegregated $C_{17}Si_3$ Heterofullerenic Isomers Using Density Functional Theory Method, *J. Chin. Chem. Soc.*, **65**:1453–1464 (2018).

(b) Haerizade B.N., Ghavami M., Koohi M., Janitabar Darzi S., Rezaee N., Kasaei M.Z., Green Removal of Toxic Pb(II) from Water by a Novel and Recyclable Ag/γ-Fe_2O_3@r-GO Nanocomposite, *Iran. J. Chem. Chem. Eng. (IJCCE)* **37(2)**:29–37 (2018).

(c) Kassaee M.Z., Buazar F., Koohi M., Heteroatom Impacts on Structure, Stability and Aromaticity of X_nC_{20-n} Fullerenes: A Theoretical Prediction, *J. Mol. Struct. (THEOCHEM)* **940**:19–28 (2010).

(d) Ghavami M., Kassaee M.Z., Mohammadi R., Koohi M., Haerizadeh B.N., Fe_2O_3@Graphene Oxide as a Novel and Effective Visible Light Photocatalyst for Removal of Rhodamine B from Water, *Solid State Sci.* **38**:143–149 (2014).

(e) Koohi M., Shariati M., Soleimani Amiri S., A Comparative Study on the Ge_6C_{14} Heterofullerene Nanocages: A Density Functional Survey, *J. Phys. Org. Chem.*, **30**:e3678–3687 (2017).

(d) Koohi M., Soleimani-Amiri S., Shariati M., Novel X- and Y-Substituted Heterofullerenes $X_4Y_4C_{12}$ Developed from the Nanocage C_{20}, where X = B, Al, Ga, Si and Y = N, P, As, Ge: a Comparative Investigation on their Structural, Stability, and Electronic Properties at DFT, *Struct. Chem.* **29(3)**: 909–920 (2018).

[4] (a) Ghavami M., Mohammadi R., Koohi M., Kassaee M.Z., Visible Light Photocatalytic Activity of Reduced Graphene Oxidesynergistically Enhanced By Successive Inclusion of γ-Fe_2O_3, TiO_2, and Ag Nanoparticles, *Mater. Sci. Semicond. Process.* **26**: 69–78 (2014).

(b) Ghavami M., Koohi M., Kassaee M.Z., A Selective Nanocatalyst for an Efficient Ugi Reaction:Magnetically Recoverable $Cu(acac)_2/NH_2$-T/SiO_2@Fe_3O_4 NPs, *J. Chem. Sci.*, **125**: 1347–1357 (2013).

(c) Ghavami M., Koohi M., Ahmadi A., Zandi H., Kassaee M.Z., Diastereoselective Synthesis of *N*-(*p*-Tosylsulfonyl)-2-Phenylaziridine Over a Novel Magnetically Recyclable Cu(II) Catalyst Accompanied with the *N*-Inversion Assessment at DFT, *Comb. Chem. High. T. Scr.* **17**:756–762 (2014).

[5] (a) Koohi M., Kassaee M.Z., Ghavami M., Haerizade B.N., Ahmadi A.A., $C_{20-n}Ge_n$ Heterofullerenes (n = 5 - 10) on Focus: A Density Functional Perspective, *Monatsh. Chem.*, **146**:1409–1417 (2015).

(b) Koohi M., Soleimani Amiri S., Shariati M., Silicon Impacts on Structure, Stability and Aromaticity of $C_{20-n}Si_n$ Heterofullerenes (n = 1 - 10): A Density Functional Perspective, *J. Mol. Struct.* **1127**:522–531 (2017).

(c) Baei M.T., Koohi M., Shariati M., Structure, Stability, And Electronic Properties of AlP Nanocages Evolved from the World's Smallest Caged Fullerene C_{20}: A Computational Study at DFT, *J. Mol. Struct.*, **1159**:118–134 (2018).

[6] (a) Hassanpour A., Youseftabar-Miri L., Delir Kheirollahi Nezhad P., Ahmadi S., Ebrahimiasl S., Kinetic Stability, and NBO Analysis of the $C_{20-n}Al_n$ Nanocages (n = 1 - 5) Using DFT Investigation, *J. Mol. Struct.*, **1233**:130079–130095 (2021).

(b) Hassanpour A., Yasar S., Ebadi A.G., Ebrahimiasl S., Ahmadi S., Thermodynamic Stability, Structural and Electronic Properties for the $C_{20-n}Al_n$ Heterofullerenes (n = 1 - 5): A DFT Study, *J. Mol. Model.*, **27(5)**: 124–135 (2021).

(c) Hassanpour A., Delir Kheirollahi Nezhad P., Hosseinian A., Ebadi A.G., Ahmadi S., Ebrahimiasl S., Characterization of IR Spectroscopy, APT Charge, ESP Maps and AIM Analysis of C_{20} and its $C_{20-n}Al_n$ Heterofullerene Analogous (n = 1 - 5) Using DFT, *J. Phys. Org. Chem.*, **34(7)**:e4198–4212 (2021).

(d) Vessally E., Soleimani–Amiri S., Hosseinian A., Edjlali L., Bekhradnia A., A Comparative Computational Study on the BN Ring Doped Nanographenes, *Appl. Surf. Sci.* **396**:740–745 (2017).

[7] (a) Bertau M., Wahl F., Weiler A., Scheumann K., Worth J., Keller M., Prinzbach H., From Pagodanes to Dodecahedranes - Search for a Serviceable Access to the Parent ($C_{20}H_{20}$) Hydrocarbon, *Tetrahedron*, **53**: 10029 (1997).

(b) Prinzbach H., Weller A., Landenberger P., Wahl F., Worth J., Scott L.T., Gelmont M., Olevano D., Issendorff B., Gas-Phase Production and Photoelectron Spectroscopy of the Smallest Fullerene, C_{20}. Nature **407**:60 (2000).

[8] (a) Liu P., Zhang H., Cheng X., Tang Y., Ti-Decorated B_{38} fullerene: A High Capacity Hydrogen Storage Material, *Int. J. Hydrogen Energy*, **41**: 19123 (2016).

(b) Dong H., Hou T., Lee S-T., Li Y., New Ti-Decorated B_{40} Fullerene as a Promising Hydrogen Storage Material, *Scientific Reports*, **5**: 9952 (2015).

(c) Dunk P.W., Kaiser N.K., Mulet-Gas M., Rodríguez-Fortea A., Poblet J.M., Shinohara H., Hendrickson C.L., Marshall A.G., Kroto H.W., The Smallest Stable Fullerene, M@C_{28} (M = Ti, Zr, U): Stabilization and Growth from Carbon Vapor, *J. Am. Chem. Soc.*, **134**: 9380 (2012).

[9] (a) Boruah B., Kalita B., Exploring Enhanced Hydrogen Adsorption on Ti Doped Al Nanoclusters: A DFT Study, *Chem. Phys.*, **518**: 123 (2019).

(b) Yildirim T., Ciraci S., Titanium-Decorated Carbon Nanotubes as a Potential High-Capacity Hydrogen Storage Medium, *Phys. Rev. Lett.*, **94**: 175501-1 (2005).

(c) Sun Q., Wang Q., Jena P., Kawazoe Y., Clustering of Ti on a C_{60} Surface and Its Effect on Hydrogen Storage, *J. Am. Chem. Soc.* **127**:14582 (2005).

[10] (a) Vessally E., Behmagham F., Massoumi B., Hosseinian A., Edjlali L., Carbon Nanocone as an Electronic Sensor for HCl Gas: Quantum Chemical Analysis, *Vacuum*, **134**: 40 (2016).

(b) Bashiri S., Vessally E., Bekhradnia A., Hosseinian A., Edjlali L., Utility of Extrinsic [60] Fullerenes as Work Function Type Sensors for Amphetamine Drug Detection: DFT Studies, *Vacuum*, **136**:156 (2017).

(c) Behmagham F., Vessally E., Massoumi B., Hosseinian A., Edjlali L., A Computational Study on the SO_2 Adsorption by the Pristine, Al, and Si Doped BN Nanosheets, *Superlattices Microstruct*, **100**: 350 (2016).

[11] (a) Cao Y., Ebadi A.G., Rahmani Z., Poor Heravi M.R., Vessally E., Substitution Effects *via* Aromaticity, Polarizability, APT, AIM, IR Analysis and Hydrogen Adsorption in $C_{20-n}Ti_n$ Nanostructures: A DFT Survey, *J. Mol. Model.*, **27**: 348–358 (2021).

(b) Kareem R.T., Ahmadi S., Rahmani Z., Ebadi A.G., Ebrahimiasl S., Characterization of titanium Influences on Structure and Thermodynamic Stability of Novel $C_{20-n}Ti_n$ Nanofullerenes (n = 1 - 5): A Density Functional Perspective, *J. Mol. Model.* **27(6)**:176–187 (2021).

[12] (a) Becke A.D., Density-Functional Exchange-Energy Approximation with Correct Asymptotic Behavior, *Phys. Rev. A* **38**:3098–3100 (1988).

(b) Becke A.D., Density-Functional Thermochemistry. III. The Role of Exact Exchange, *J. Chem. Phys.* **98**:5648–5652 (1993).

(c) Becke A.D., Density-Functional Thermochemistry. IV. A New Dynamical Correlation Functional and Implications for Exact-Exchange Mixing, *J. Chem. Phys.* **104**:1040–1046 (1996).

(d) Lee C., Yang W., Parr R.G., Development of the Colle-Salvetti Correlation-Energy Formula into a Functional of the Electron Density, *Phys. Rev. B* **37**: 785–789 (1988).

(e) Zhao Y., Truhlar D.G., The M06 Suite of Density Functionals for Main Group Thermochemistry, Thermochemical Kinetics, Noncovalent Interactions, Excited States, and Transition Elements: Two New Functionals and Systematic Testing of Four M06-Class Functionals and 12 oOther Functionals, *Theor. Chem. Account.*, **120**: 215 (2008).

[13] (a) Schmidt M.W., Baldridge K.K., Boatz J.A., Elbert S.T., Gordon M.S., Jensen J.H., Koseki S., Matsunaga N., Nguyen K.A., Su S.J., Windus T.L., Dupuis M., Montgomery J.A., General Atomic and Molecular Electronic Structure System, *J. Comput. Chem.*, **14(11)**:1347–1363 (1993).

(b) Sobolewski A.L., Domcke W., *Ab Initio* Investigation of the Structure and Spectroscopy of Hydronium−Water Clusters, *J. Phys. Chem. A* **106**: 4158–4167 (2002).

[14] (a) Hariharan P.C., Pople J.A., Accuracy of AH_n equilibrium Geometries by Single Determinant Molecular Orbital Theory, *J. Mod. Phys.*, **27**: 209–214 (1974).

(b) Francl M.M., Pietro W.J., Hehre W.J., Binkley J.S., Gordon M.S., DeFrees D.J., Pople J.A., Self-Consistent Molecular Orbital Methods. XXIII. A Polarization-Type Basis Set for Second Row Elements, *J. Chem. Phys.*, **77**: 3654-3665 (1982).

(c) Frisch M.J., Pople J.A., Binkley J.S., Self-Consistent Molecular Orbital Methods 25: Supplementary Functions for Gaussian Basis Sets, *J. Chem. Phys.*, **80**: 3265–3269 (1984).

(d) Clark T., Chandrasekhar J., Spitznagel G.W., Schleyer P.v.R., Efficient Diffuse Function-Augmented Basis Sets for Anion Calculations. III. The 3-21+G set for First-Row Elements, Li-F, *J. Comput. Chem.*, **4**: 294–301 (1983).

[15] (a) Glendening E.D., Reed A.E., Carpenter J.E., Weinhold F., "NBO Version 3.1" Gaussian Inc., Pittsburgh. (2003).

(b) Weinhold F., Natural Bond Orbital Analysis: A Critical Overview of Relationships to Alternative Bonding Perspectives, *J. Comput. Chem.* **33**: 2363 (2012).

(c) Glendening ED, Landis CR, Weinhold F., Natural Bond Orbital Methods, *Wiley Interdiscip Rev. Comput. Mol. Sci.*, **2**: 1 (2012).

(d) Zhang G., Musgrave C.B. Comparison of DFT Methods for Molecular Orbital Eigenvalue Calculations, *J. Phys. Chem. A*, **111**: 1554 (2007).

[16] Predew J.P., Wang Y., Accurate and Simple Analytic Representation of the Electron-Gas Correlation Energy, *Phys. Rev. B*, **45**: 13244(1992).

[17] (a) Domingo L.R., Chamorro E., Pérez P., Understanding the Reactivity of Captodative Ethylenes in Polar Cycloaddition Reactions. A Theoretical Study, *J. Org. Chem.*, **73**: 4615 (2008).

(b) Parr R.G., Szentpaly L., Liu S., Electrophilicity Index, *J. Am. Chem. Soc.*, **121**:1922 (1999).

(c) Parr R.G., Pearson R.G., Absolute Hardness: Companion Parameter to Absolute Electronegativity, *J. Am. Chem. Soc.*, **105**:7512(1983).

(d) Parr R.G., Yang W., "Density Functional Theory of Atoms and Molecules", Oxford University Press, New York (1989).

[18] Zhang G., Musgrave C.B., Comparison of DFT Methods for Molecular Orbital Eigenvalue Calculations, *J Phys Chem A*, **111**: 1554 (2007).

[19] (a) Gharibzadeh F., Vessally E., Edjlali L., Es'haghi M., Mohammadi R., A DFT Study on Sumanene, Corannulene and Nanosheet as the Anodes in Li−Ion Batteries, *Iran. J. Chem. Chem. Eng. (IJCCE)*, **39(6)**: 51-62 (2020).

(b) Afshar M., Khojasteh R.R., Ahmadi R., Nakhaei Moghaddam M., In Silico Adsorption of Lomustin Anticancer Drug on the Surface of Boron Nitride Nanotube, *Chem. Rev. Lett.*, **4**:178−184 (2021).

(c) Vessally E., Hosseinian A., A Computational Study on the Some Small Graphene-Like Nanostructures as the Anodes in Na−Ion Batteries, *Iran. J. Chem. Chem. Eng. (IJCCE)*, **40(3)**:691-703 (2021).

(d) Hashemzadeh B., Edjlali L., Delir Kheirollahi Nezhad P., Vessally E., A DFT Studies on a Potential Anode Compound for Li-Ion Batteries: Hexa-Cata-Hexabenzocoronene Nanographen, *Chem. Rev. Lett.*, **4**:232-238 (2021).

(e) Mohammadi M., Siadati S. A., Ahmadi S., Habibzadeh S., Poor Heravi M.R., Hossaini Z., Vessally E., Carbon Fixation of CO_2 Via Cyclic Reactions with Borane in Gaseous Atmosphere Leading to Formic Acid (And Metaboric Acid); a Potential Energy Surface (PES) Study, *Front. Chem.*, **10** (2022).

[20] (a) Vessally E., Farajzadeh P., Najaf, E., Possible Sensing Ability of Boron Nitride Nanosheet and Its Al– and Si–Doped Derivatives for Methimazole drug by Computational Study, *Iran. J. Chem. Chem. Eng. (IJCCE)*, **40(4)**: 1001-1011 (2021).

(b) Majedi S., Sreerama L., Vessally E., Behmagham F., Metal-Free Regioselective Thiocyanation of (Hetero) Aromatic C-H Bonds Using Ammonium Thiocyanate: An Overview, *J. Chem. Lett.*, **1**: 25-31 (2020).

(c) Salehi N., Vessally E., Edjlali L., Alkorta I., Eshaghi M., Nan@Tetracyanoethylene (n=1-4) Systems: Sodium Salt Vs Sodium Electride, *Chem. Rev. Lett.*, **3**: 207-217 (2020).

(d) Soleimani-Amiri S., Asadbeigi N., Badragheh S., A Theoretical Approach to New Triplet and Quintet (nitrenoethynyl) alkylmethylenes,(nitrenoethynyl) alkylsilylenes,(nitrenoethynyl) alkylgermylenes, *Iran. J. Chem. Chem. Eng. (IJCCE)*, **39(4)**: 39-52 (2020).

[21] (a) Sreerama L., Vessally E., Behmagham F., Oxidative Lactamization of Amino Alcohols: An Overview, *J. Chem. Lett.*, **1**: 9-18 (2020).

(b) Norouzi N., Ebadi A. G., Bozorgian A., Vessally E., Hoseyni S. J., Energy and Exergy Analysis of Internal Combustion Engine Performance of Spark Ignition for Gasoline, Methane, and Hydrogen Fuels, *Iran. J. Chem. Chem. Eng. (IJCCE)*, **40(6)**: 1909-1930 (2021).

(c) Kamel M., Mohammadifard, M., Thermodynamic and Reactivity Descriptors Studies on the Interaction of Flutamide Anticancer Drug with Nucleobases: A Computational View, *Chem. Rev. Lett.*, **4**: 54-65 (2021).

(d) Vessally E., Musavi M., Poor Heravi M.R., A Density Functional Theory Study of Adsorption Ethionamide on The Surface of the Pristine, Si and Ga and Al-Doped Graphene, *Iran. J. Chem. Chem. Eng. (IJCCE)*, **40(6)**: 1720-1736 (2021).

[22] (a) Vakili M., Bahramzadeh V., Vakili M., A Comparative study of SCN- adsorption on the $Al_{12}N_{12}$, $Al_{12}P_{12}$, and Si and Ge -doped $Al_{12}N_{12}$ nano-cages to remove from the environment, *J. Chem. Lett.* 1:172−178 (2020).

(b) Norouzi N., Ebadi A. G., Bozorgian A., Hoseyni S.J., Vessally E., Cogeneration System of Power, Cooling, and Hydrogen from Geothermal Energy: An Exergy Approach, *Iran. J. Chem. Chem. Eng. (IJCCE)*, **41(2)**: 706-721 (2022).

(c) Mosavi M., Adsorption Behavior of Mephentermine on the Pristine and Si, Al, Ga- Doped Boron Nitride Nanosheets: DFT Studies, *J. Chem. Lett.*, **1**: 164-171 (2020).

(d) Vessally E., Siadati S.A., Hosseinian A., Edjlali L., Selective Sensing of Ozone and the Chemically Active Gaseous Species of the Troposphere by Using the C20 Fullerene and Graphene Segment, *Talanta*, **162**: 505-510 (2017).

[23] (a) Norouzi N., Ebadi A. G., Bozorgian A., Hoseyni S.J., Vessally E., Cogeneration System of Power, Cooling, and Hydrogen from Geothermal Energy: An Exergy Approach, *Iran. J. Chem. Chem. Eng. (IJCCE)*, **41(2)**: 706-721 (2022).

(b) Rabipour S., Mahmood E.A., Afsharkhas M., A Review on the Cannabinoids Impacts on Psychiatric Disorders, *Chem. Rev. Lett.*, **5**: (2022).

(c) Siadati S.A., Vessally E., Hosseinian A., Edjlali L., Possibility of Sensing, Adsorbing, and Destructing the Tabun-2D-Skeletal (Tabun Nerve Agent) by C20 Fullerene and its Boron and Nitrogen Doped Derivatives, *Synthetic Metals*, **220**: 606-611 (2016).

(d) Rabipour S., Mahmood E.A., Afsharkhas M., Medicinal Use of Marijuana and its Impacts on Respiratory System, *J. Chem. Lett.*, **3**: 86-94 (2022).

[14] (a) Bader R.F.W., The Quantum Mechanical Basis of Conceptual Chemistry, *Monatsh. Chem.*, **136**: 819 (2005).
(b) Biegler–König F., Schönbohm J., Update of the AIM2000-Program for Atoms in Molecules, *J. Comp. Chem.*, **23**:1489 (2002).

[25] (a) Froudakis G.E., "Why Alkali-Metal-Doped Carbon Nanotubes Possess High Hydrogen Uptake", *Nano. Lett.*, **1**: 531 (2001).
(b) Mavrandonakis A., Froudakis G.E., Schnell M., Muhlhauser M., from Pure Carbon to Silicon Carbon Nanotubes: an *ab initio* Study, *Nano. Lett.*, **3**: 1481 (2003).
(c) Mpourmpakis G., Froudakis G.E., Lithoxoos G.P., Samios J., SiC Nanotubes: A Novel Material for Hydrogen Storage, *Nano. Lett.*, **6**: 1581 (2006).